NATIONAL ADVISORY COMMITTEE FOR AERONAUTICS

TECHNICAL NOTE 3881

WIND-TUNNEL TECHNIQUE FOR SIMULTANEOUS SIMULATION OF EXTERNAL FLOW FIELD ABOUT NACELLE INLET AND EXIT AIRSTREAMS AT SUPERSONIC SPEEDS

By Gerald W. Englert and Roger W. Luidens

Lewis Flight Propulsion Laboratory
Cleveland, Ohio

Washington
January 1957

NATIONAL ADVISORY COMMITTEE FOR AERONAUTICS

TECHNICAL NOTE 3881

WIND-TUNNEL TECHNIQUE FOR SIMULTANEOUS SIMULATION OF EXTERNAL FLOW FIELD ABOUT NACELLE INLET AND EXIT AIRSTREAMS AT SUPERSONIC SPEEDS

By Gerald W. Englert and Roger W. Luidens

SUMMARY

An investigation was made of several ways of simultaneously simulating the external pressure field generated by an engine exhaust jet and an air inlet. The techniques investigated used high-pressure air piped upstream through the simulated jet to the exhaust nozzle of the engine. It was then discharged through perforations in the pipe or in a downstream direction through a target-type reverser at the end of the pipe. This air combined with the engine-inlet air to form a jet contour. The tests were made at free-stream Mach numbers of 2.5 and 3.0 for a range of jet-exit static-pressure ratios from 1.0 to 3.0.

The results of the study indicated that the pressure field in the vicinity of the exit station and external to a real exhaust jet could be adequately simulated while keeping the inlet at critical or supercritical mass flow. The techniques of this report then provide a simple means of simulating inlet and exit interference effects in wind-tunnel investigations of airplane configurations.

INTRODUCTION

The forces and moments in many configurations of supersonic airplanes are influenced by interference effects from both the engine inlet and the exhaust nozzle. For instance, the importance of jet-interference effects is demonstrated in references 1 and 2. Figure 1(a) shows an example of an airplane where significant portions of that airplane are subject to interference effects caused by the engine air intake system and the exhaust jet. The airplane forces and moments will hence be affected by these interference effects. These effects are not amenable to calculation and should be duplicated in wind-tunnel tests. Because of the small size of most wind-tunnel models of airplane configurations, duplicating the actual total-temperature and -pressure ratios across the airplane engine is impractical or impossible. If these ratios are not attained, the ratios of exhaust-nozzle throat area to minimum inlet area are not matched to furnish proper inlet operation and the desired amount of expansion in the nozzle. The problem is further complicated by the condition that the model should be kept free of foreign forces and flow disturbances.

A technique suitable for wind-tunnel studies for simulating the pressure field in the vicinity of an exhaust jet and simultaneously representing inlet flow conditions typical of critical or supercritical operation is experimentally investigated in this report. In this technique high- 4197
pressure air is piped upstream through the exhaust jet and discharged in such a way as to duplicate the displacement of the real jet. Several methods of distributing the additional air are investigated. Comparisons are made of the pressure distributions generated by real and simulated exhaust jets on a test body. Simulation of the actual engine cowl contour is all that is needed to simulate the inlet interference field at critical or supercritical operation.

No attempt was made to simulate the effects of the jet shock (ref. 3), which occurs further downstream within the jet and then passes out through the external flow at supersonic flight speeds. However, this shock is too far downstream to affect airplane performance for many configurations.

SYMBOLS

The following symbols are used in this report:

A cross-sectional area

C pressure coefficient, $\frac{p - p_0}{q_0}$

l axial distance from start of enlarged internal flow area of nacelle to nacelle trailing edge

M free-stream Mach number

n number of holes

P total pressure

p static pressure

q dynamic pressure, $\frac{\gamma}{2} pM^2$

r radius from nacelle centerline

T total temperature of air flowing through probe

w weight flow of air through probe

x distance along axis of perforated probe downstream of cone cylinder juncture

α distance tube is immersed in target

β distance between trailing edges of target and nacelle

γ ratio of specific heats for air

ν Prandtl-Meyer expansion angle

θ angle between hole axis and tube axis on perforated probe

Subscripts:

av average

e nozzle exit

i 1^{st}, 2^{nd}, 3^{rd} . . . row of holes

p probe

t total

0 free stream

1 target trailing-edge station

3 farthest downstream axial station in jet

$*$ refers to conditions where Mach number equals 1

APPARATUS AND MODELS

Wind Tunnel

The investigation was conducted at the NACA in the Lewis laboratory 1- by 1-foot block tunnel operated at a Mach number of 2.5 with an inlet total pressure of 7.5 pounds per square inch absolute and at a Mach number of 3.0 at atmospheric inlet pressure. The stagnation temperature was set at 100° F. The specific humidity was maintained sufficiently low to make condensation effects negligible.

Jet Simulation Considerations

Figure 1(b) shows the application and approach to the problem of simulating both the inlet and the exhaust systems considered in this report. The airplane is mounted from a sting, and the forces and moments on the airplane are measured with the internal balance. The engine internal contours that exist in the real airplane are replaced by a simple cylindrical section (section C). The external inlet lip and the nacelle shape are maintained to duplicate correctly the inlet pressure field at critical or supercritical operation. The internal passage is enlarged to the maximum nozzle-exit diameter by a step at section D, where the base pressure must be measured and the corresponding force subtracted from the balance measurement. In order to simulate the external pressure field of the exhaust jet, high-pressure air is brought in through a pipe and exhausted through a target-type reverser that is internal to the nacelle. There should be no mechanical interference binding between the airplane model and the probe that would introduce extraneous forces into the balance measurements.

4197

Models

The ability to simulate the flow field about the exhaust jet was determined by comparison of pressure measurements made on a half-cylinder mounted near actual and simulated jets. The dimensions of the configuration that provides for what is termed in this report the "real" jet are shown in figure 2(a). High-pressure air is fed through holes in the support strut to the plenum chamber within the model and exhausted through the convergent-divergent nozzle. Figure 2(b) presents the details of the nacelle for which it is desired to simulate the field about the inlet and the exhaust jet. The internal contours are cylindrical for ease of force measurements in future applications. The maximum diameter of both the real jet model and the nacelle model is 2 inches. Because the present tests required only static-pressure measurements, the strut between the probes and nacelle is permissible; but it probably could have been deleted leaving no extraneous mechanical forces.

Two different type probes, perforated and target, were used to inject the additional air required within the nacelle to control the jet boundary and, in turn, generate the corresponding external flow field. The perforated probes (fig. 3(a)) distributed the air along the jet centerline by means of specified hole locations in the probe wall. A prescribed jet displacement contour should then be attained. The target probes (fig. 3(b)), however, created a specified static pressure of the exhaust air at the nozzle-exit station. Downstream of the exit the air should form a proper jet boundary with no more guidance.

Perforated Probes

The probes were designed primarily to simulate the jet boundary downstream of the convergent-divergent nozzle of figure 2(a) when operating underexpanded at an average ratio of jet-exit static pressure to free-stream static pressure of 2.0 and at a free-stream Mach number of 3.

Previous data were inspected to estimate a jet boundary at these conditions (fig. 4). The cross-sectional area of this jet stream was then computed as a function of axial distance downstream of the nacelle internal shoulder where the flow passage was enlarged. Except for the constant-area section downstream of this shoulder, the holes were arbitrarily spaced at either 0.15- or 0.3-nozzle-exit-diameter intervals along the tube axis (fig. 3(a)). The hole size was selected small enough so that a reasonable number could be drilled to simulate axisymmetric flow and yet not too small to drill with ordinary methods. The total number of holes was then determined to pass the required total rate of jet weight flow to fill the jet stream minus the nacelle inlet flow. This calculation used the pressure and temperature supplied to the probe from the laboratory supply. It was assumed that the average Mach number inside the nacelle and in the jet stream was equal to the free-stream value, since ahead of the probe the internal passage was of constant cross section and the flow was supersonic. The number of holes at each station was set according to the following equation (see fig. 5(a)):

$$\begin{array}{l}\text{Number of}\\ \text{holes at each}\\ \text{axial station}\end{array} = \frac{(\text{Total number of holes})\left(\begin{array}{l}\text{Increase of jet cross-sectional}\\ \text{area over that at previous row}\\ \text{of holes}\end{array}\right)}{\left(\begin{array}{l}\text{Total cross-sectional area}\\ \text{at maximum jet diameter}\\ \text{considered}\end{array}\right) - \left(\begin{array}{l}\text{Nacelle inlet plus probe}\\ \text{cross-sectional area}\end{array}\right)}$$

or

$$n_i = \frac{n_t\left(\pi r_i^2 - \pi r_{i-1}^2\right)}{\pi r_3^2 - \pi r_0^2 - \pi r_p^2} = \frac{n_t\left(r_i^2 - r_{i-1}^2\right)}{r_3^2 - r_0^2 - r_p^2}$$

Disturbances were assumed to propagate outward from the holes along the Mach cones.

When 0.020-inch-diameter holes were used, there were sometimes too many holes for the tube circumference. At these stations, therefore, two rows of holes were made, each with a slight axial displacement from the other.

Differences between the actual and estimated average angle of propagation of flow disturbance produced by the air bleed from the probe could be somewhat compensated for by translating the probe along its axis.

The holes in the first probe were drilled normal to the tube surface. The holes in the second probe were drilled at 30° with respect to the probe axis and were directed downstream. The total hole area and the distribution of the hole area were the same as for the first probe, but the number of holes was approximately doubled. Later in the investigation the probe hole spacing was revised using schlieren photographs of the real jet boundary rather than from the previously estimated jet boundary (fig. 4).

4197

Target Probes

The target probe (fig. 5(b)) was designed to simulate the conditions at the exit station of the real jet under the assumption that the correct jet boundary would follow from the correct conditions at the exit station. The cone angle of the target probe was kept small (9°30' half-angle) to minimize total-pressure losses in the inlet air. The probe was inserted into the nacelle far enough so that the nacelle-inlet air would be contracted to form a jet-exit static-pressure ratio p_e/p_0 of 2.0 at the model exit station. The Mach number at station 1 was computed using isentropic flow relations between stations 0 (M_0 = 3) and 1. The area and the Mach number at station e were likewise calculated to yield the desired exit pressure:

$$M_e = \sqrt{\frac{2}{\gamma - 1}\left[\left(\frac{P_0}{2p_0}\right)^{\frac{\gamma-1}{\gamma}} - 1\right]} = 2.55$$

$$A_e = \frac{(A_*/A_0)\ A_0}{A_*/A_e} = \frac{M_0 A_0}{M_e}\left(\frac{1 + \frac{\gamma - 1}{2} M_e^2}{1 + \frac{\gamma - 1}{2} M_0^2}\right)^{\frac{\gamma+1}{2(\gamma-1)}} = 1.243 \text{ sq in.}$$

By assuming that the flow is attached to the nacelle wall at station e, the radius to the inside bounding streamline r_e of the nacelle-inlet mass flow is

$$r_e = \sqrt{0.97^2 - \frac{1.243}{\pi}} = 0.739 \text{ in.}$$

It was also assumed that mixing across this bounding streamline was negligible. The average angle between stations 1 and e of this bounding streamline was then calculated. It was assumed that $\Delta r/r$ was small so that the Prandtl-Meyer relation (ref. 4) could be used for the average nacelle airstream directions between these stations:

$$\nu_1 = \sqrt{\frac{\gamma + 1}{\gamma - 1}} \tan^{-1} \sqrt{\frac{\gamma - 1}{\gamma + 1} (M_1^2 - 1)} - \left[90^\circ - \sin^{-1} \left(\frac{1}{M_1}\right)\right] = 52.3^\circ$$

$$\nu_e = 40.1^\circ$$

$$\Delta\nu_{av} = 12.2^\circ$$

The latter term was considered the average change of direction of the stream tube (see fig. 5(b)). The change of direction on the inner bounding streamline $\Delta\nu_{inner}$ is calculated as follows:

$$\Delta\nu_{av} = \frac{\Delta\nu_{inner} + \Delta\nu_{outer}}{2}$$

where

$$\Delta\nu_{outer} = 0$$

therefore;

$$\Delta\nu_{inner} = 2\Delta\nu_{av} = 24.4^\circ$$

If the flow at station 1 is in an axial direction,

$$\frac{\Delta r}{\tan \Delta\nu_{inner}} = \frac{0.739 - 0.440}{0.454} = 0.658 \approx 5/8 \text{ in.}$$

This calculation indicated that the trailing edge of the probe should be approximately 5/16 exit diameter upstream of the nacelle trailing edge. The step in the internal nacelle contour (0.97-in. rad.) was located with respect to the probe to avoid choking the internal flow and to permit the inlet to start.

Instrumentation

The instrumentation used to determine the characteristics of the real and simulated jets was the half-cylindrical surface also shown in figure 2. The leading edge of the half-cylinder was at the same axial station as the jet exit but displaced radially 1 jet-exit diameter from the centerline of the jet. The model and half-cylinder were at zero angle of attack and yaw with respect to the free stream in all tests. Static-pressure taps were located along the plane of symmetry of the half-cylinder at 1/4-inch intervals measured from the leading edge.

Static pressures were measured in the plenum chamber of the real jet and also in the probe and the nacelle in the case of the simulated jet.

Airflow rates in the real jet and through the probes were measured using standard ASME orifices.

Schlieren viewing and photography were available at both the inlet and exit of the models.

RESULTS AND DISCUSSION

Experimental Results

4197

The simulated jets were evaluated by comparing the static pressures generated on a half-cylinder by both the real and simulated jets. The data are plotted as pressure coefficient C against distance downstream of the nozzle-exit station measured in nozzle-exit diameters in figures 6 to 11. Several general observations may be made for all the results as seen, for example, in figure 6. As the jet-exit static-pressure ratio p_e/p_0 increases, the peak pressure coefficient on the half-cylinder increases and moves upstream. The disturbance measured in the present tests reaches a maximum at a distance of approximately 1.1 nozzle diameters downstream of the exit. This is the location where the shock (formed by deflection of the external air as it intersects the jet stream) strikes the half-cylinder.

Target Probe

The results for one of the better target-probe designs are presented in figures 6 and 7 for $M_0 = 3.0$ and 2.5, respectively, over a range of jet-exit static-pressure ratios from 1.00 to 2.54. The agreement between the real and simulated jets is quite good, particularly at the higher jet-exit static-pressure ratios where the jet interference would be the largest.

Several variations made in the target probe gave an idea of the sensitivity of the results to the design and location of the probe. These results are presented in figure 8 at a free-stream Mach number of 3.0 for a jet-exit static-pressure ratio of 1.94 and may also be compared with the data of figure 6(c). The original probe design had the probe located 5/16 exit diameter inside the model, and the enlarged area started 2 inches upstream of the nacelle trailing edge (see fig. 3(b)). This gave the pressure distribution shown in figure 8(a). The nacelle-inlet flow of this configuration, however, choked at $M_0 = 2.5$, which yielded poorer distributions; so several modifications were considered to avoid the choking. The first modification moved the probe out 1/8 inch. This gave the pressure distribution shown in figure 8(b). For this configuration the nacelle-inlet flow did not choke at $M_0 = 2.5$. For the second modification, the probe was 5/16 exit diameter inside the model and the step was cut 1/8 inch deeper into the model (see l, fig. 3(b)). This configuration also did not choke at $M_0 = 2.5$ and was used for the data presented in figures 6 and 7.

A third modification increased the minimum area in the probe (see α, fig. 3(b)). The primary effect of this increase was to change the pressure and mass flow required in the probe to simulate a given jet static-pressure ratio. This will be discussed in the section Pressure and Airflow Required in Probes. The pressure distribution for this case is shown in figure 8(c). In general, the pressure distributions were not affected much by the modifications considered, and the differences between the real- and simulated-jet pressure coefficients were quite small.

Perforated Probe

The results for the perforated-probe designs are presented in figures 9 to 11 for $M_0 = 3.0$ and jet-exit static-pressure ratios from 1.05 to 2.19.

In figure 9 the probe shoulder (cone cylinder juncture) is located 1.75 exit diameters upstream of the model trailing edge. This is the correct axial position if the disturbances are propagated outward at an average Mach angle corresponding to a free-stream Mach number of 3.0. The holes were normal to the probe surface. The agreement between the real and simulated jet is quite good at the jet static-pressure ratio of 1.94 (fig. 9(a)). However, at lower pressure ratios, the peak pressure coefficient of the simulated jet fell progressively further downstream of that for the real jet. Improvement was made by moving the probe farther inside the model. Typical results are shown on figure 10. Satisfactory results were obtained when the cone-cylinder juncture of the probe was at 2.43 and 2.68 exit diameters inside the model.

Revision of the probe by basing the hole distribution on the schlieren photographs of the real jet (fig. 4) made little improvement, as shown by comparing figures 9(a) and 10(c). Differences of the jet boundaries used to calculate hole distribution between the original and revised probe are shown on figure 4 to be almost within the width of the mixing-zone region between the jet and the external flow. The revised probe had essentially more hole area near the upstream portion of the probe (fig. 3(a)).

Slanting the probe holes back from normal to 30° with respect to the probe surface (fig. 11) made very little difference in the pressure distributions. Improvement due to revision of the hole spacing corresponding to the revision on figure 9 is shown in figure 11(b).

Pressure and Airflow Required in Probes

The total pressure, as a fraction of the free-stream total pressure, required in the probe to simulate various jet-exit static-pressure ratios is shown in figure 12. In all cases the total pressure in a given probe must be increased to simulate increasing jet-exit static-pressure ratios. Also the total pressure required by the target-type probes is markedly higher than required by the perforated probes. For the target probes, increasing the minimum area in the probe decreased the required total pressure in the probe. At $M_0 = 2.5$ the required probe to free-stream total-pressure ratio was higher than at $M_0 = 3.0$. 4197

Slanting the holes of the perforated probes increased the required total pressure in the probe to simulate a given jet-exit static-pressure ratio.

The weight flow of air required by the various probes as a function of jet-exit static-pressure ratio is shown in figure 13. These curves follow the same trend as the total-pressure curves because the probe-outlet throat areas were always choked for this investigation.

CONCLUDING REMARKS

An investigation of two techniques to simulate the pressure field generated by the exhaust jet of an engine while simultaneously representing critical operation of the inlet was made at free-stream Mach numbers of 2.5 and 3.0. The results indicated that the use of high-pressure air piped upstream through the simulated jet and discharged either through perforations or a target-type reverser at the end of the pipe can be made to simulate adequately the pressure field of a real jet in the vicinity of the jet exit.

Preliminary information to determine the jet boundaries for the nozzle and pressure ratios to be simulated must be available for use in designing the perforated probes. A means, such as a small pilot model, of determining the probe weight flows must also be available for both probes if the method is to be used beyond the range of variables studied in this report.

The method may also be used to considerable advantage in jet-exit studies in a large supersonic wind tunnel which has an insufficient amount of high-pressure air to supply the nozzle of large models in the conventional manner. The limited amount of air would first supply a small pilot model and then supply probe air in the following large-model investigation.

Lewis Flight Propulsion Laboratory
National Advisory Committee for Aeronautics
Cleveland, Ohio, November 2, 1956

REFERENCES

1. Squire, H. B.: Jet Flow and Its Effects on Aircraft. Aircraft Eng., vol. XXII, no. 253, Mar. 1950, pp. 62-67.

2. Falk, H.: The Influence of the Jet of a Propulsion Unit on Nearby Wings. NACA TM 1104, 1946.

3. Courant, R., and Friedrichs, K. O.: Supersonic Flow and Shock Waves. Interscience Pub., Inc., 1948.

4. Ames Research Staff: Equations, Tables, and Charts for Compressible Flow. NACA Rep. 1135, 1953. (Supersedes NACA TN 1428.)

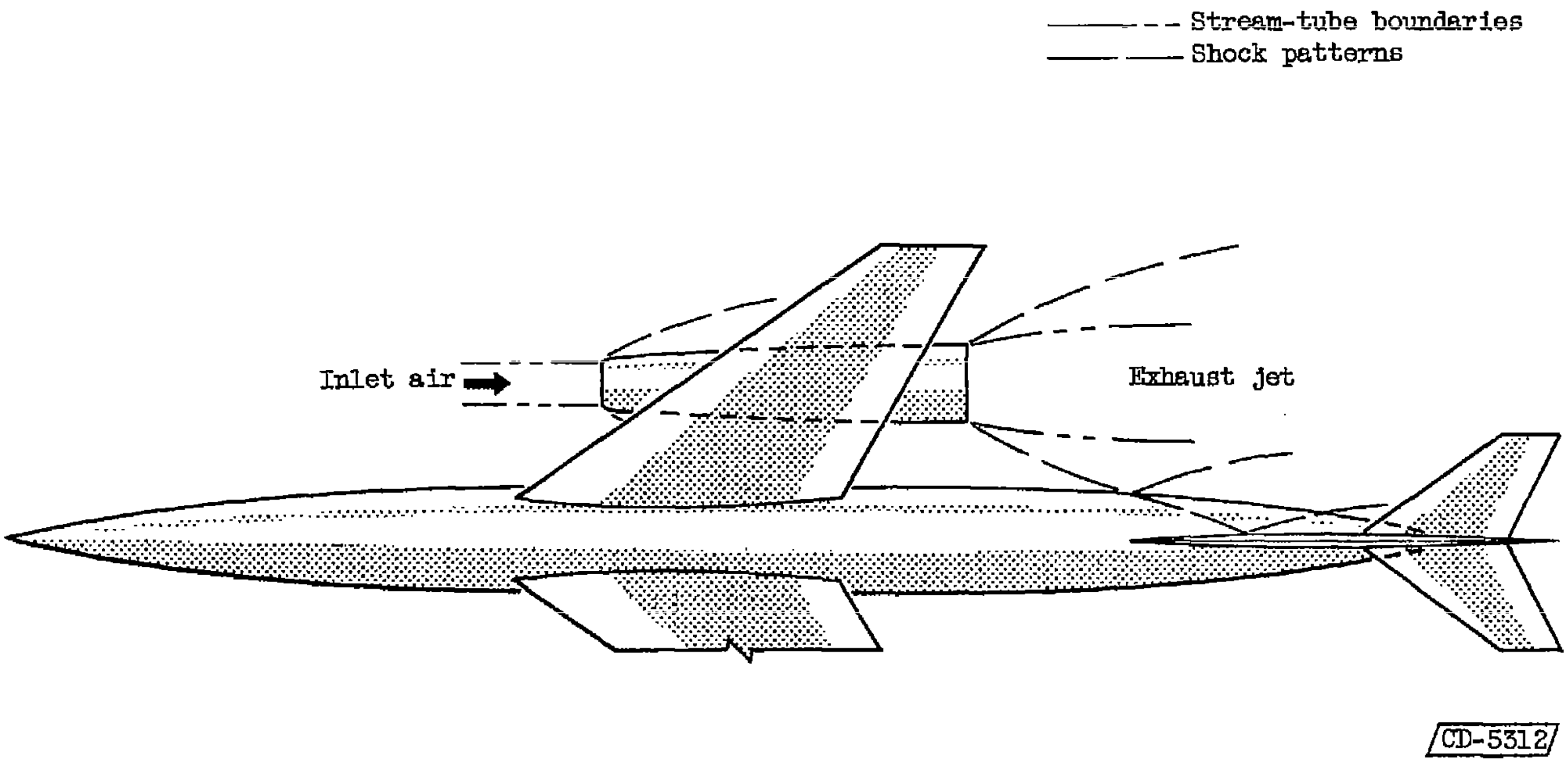

(a) Actual airplane interference due to inlet and exit.

Figure 1. - Airplane interference problem.

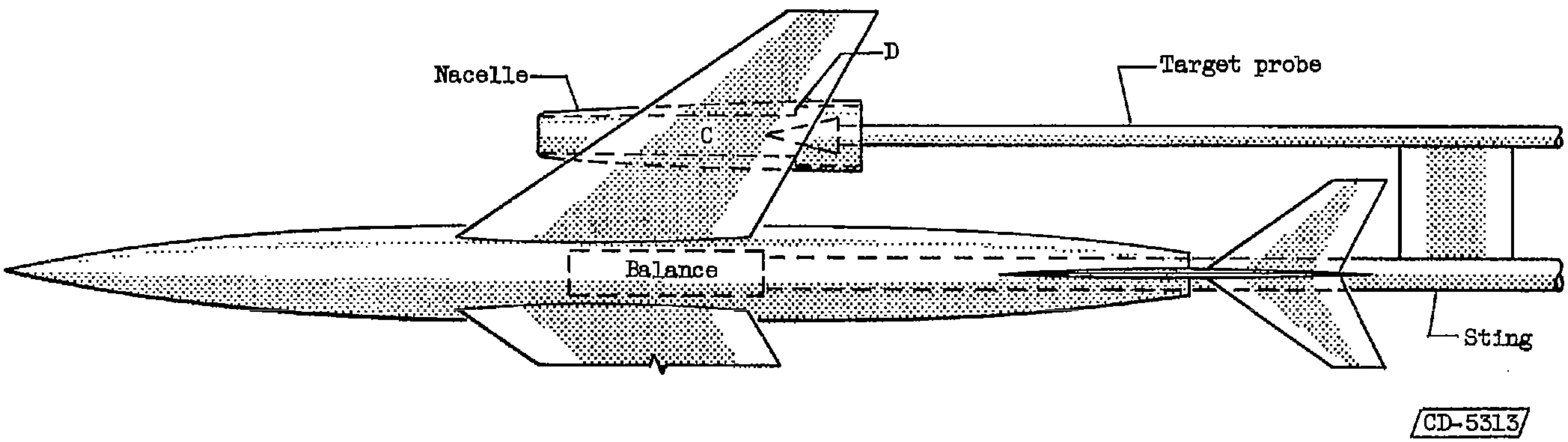

(b) Model airplane installation.

Figure 1. - Concluded. Airplane interference problem.

4197

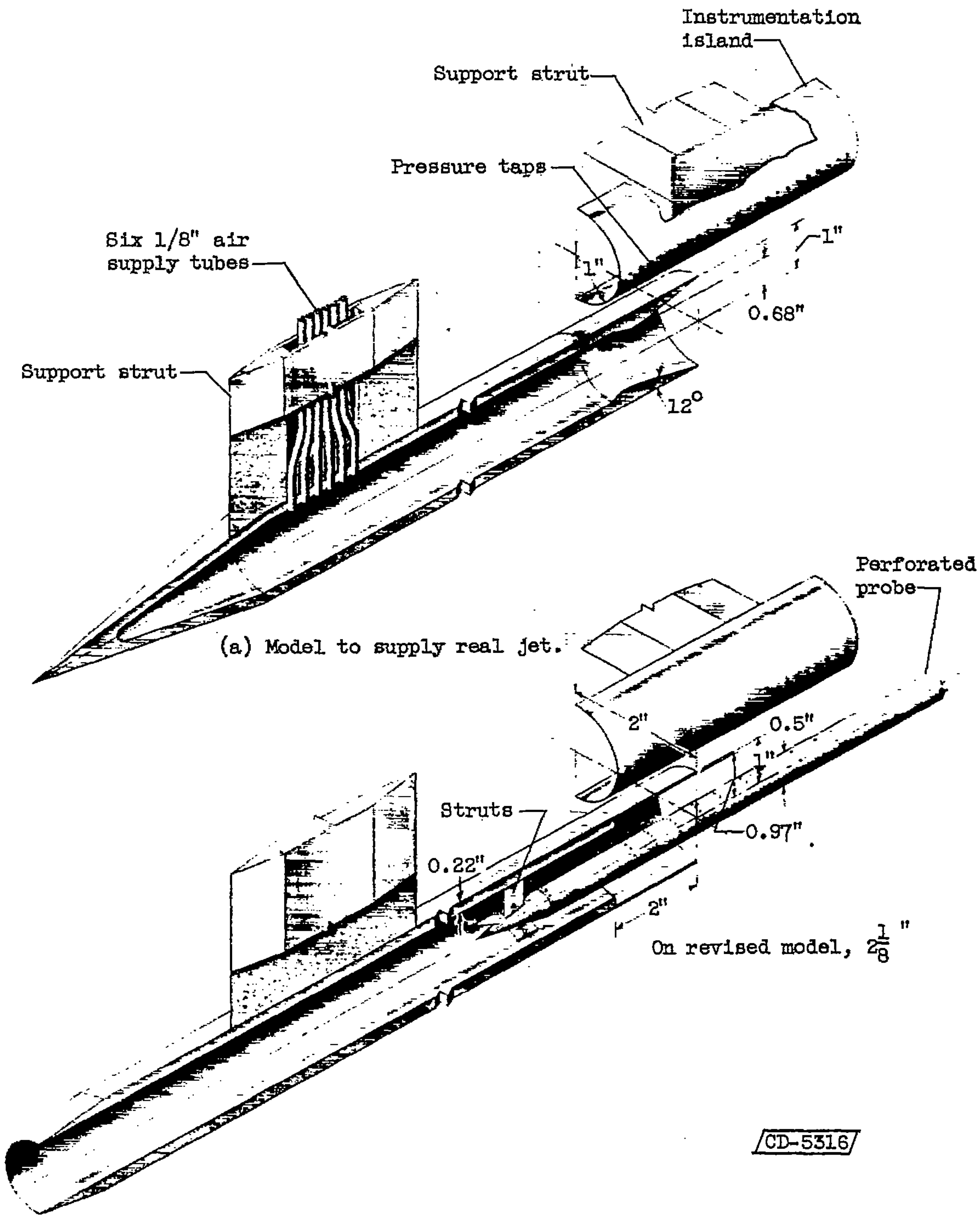

(a) Model to supply real jet.

(b) Model to simulate inlet and jet streams.

Figure 2. - Nacelle models.

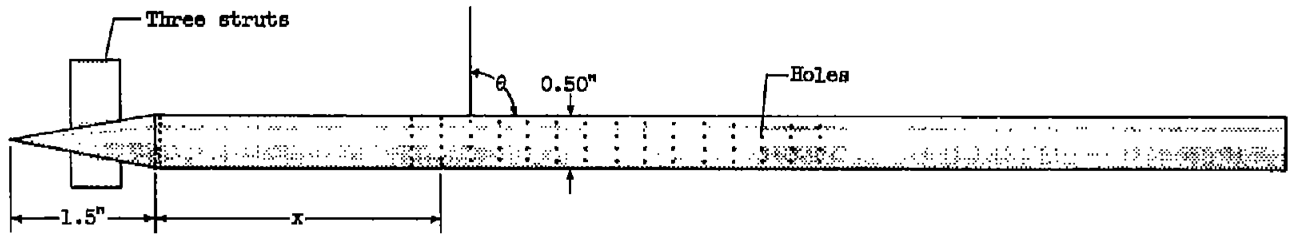

Angle between hole axis and tube axis, θ, 90°																					
x, in.		0.10	0.20	1.71	1.81	2.06	2.36	2.66	2.96	3.26	3.56	3.86	4.16	4.46	4.76	5.06	5.36	5.66	6.26	6.86	Hole diam. in.
No. of holes	Original	13						11		11		11		10		7		6	4	2	0.051
	Revised	37	37	40	40	52	49	35	42	25	24	18	20	24	18	7	10	3			0.020

θ, 30°																					
x, in.		0.10	1.76	2.06	2.36	2.66	2.96	3.26	3.56	3.86	4.16	4.46	4.76	5.06	5.36	5.66	5.96	6.26	6.56	6.86	Hole diam. in.
No. of holes	Original	27				11	11	11	11	11	11	10	9	8	7	6	5	5	4	4	0.0353
	Revised	24	25	17	16	11	14	8		13		14		8		4					0.0353

(a) Perforated probe

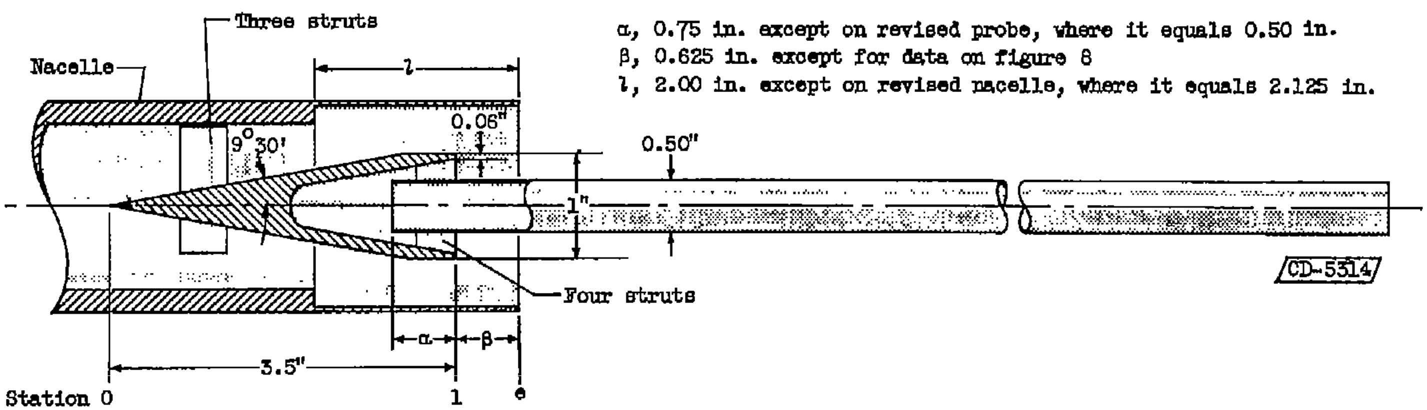

(b) Target probe.

Figure 3. - Probe for controlling jet boundary.

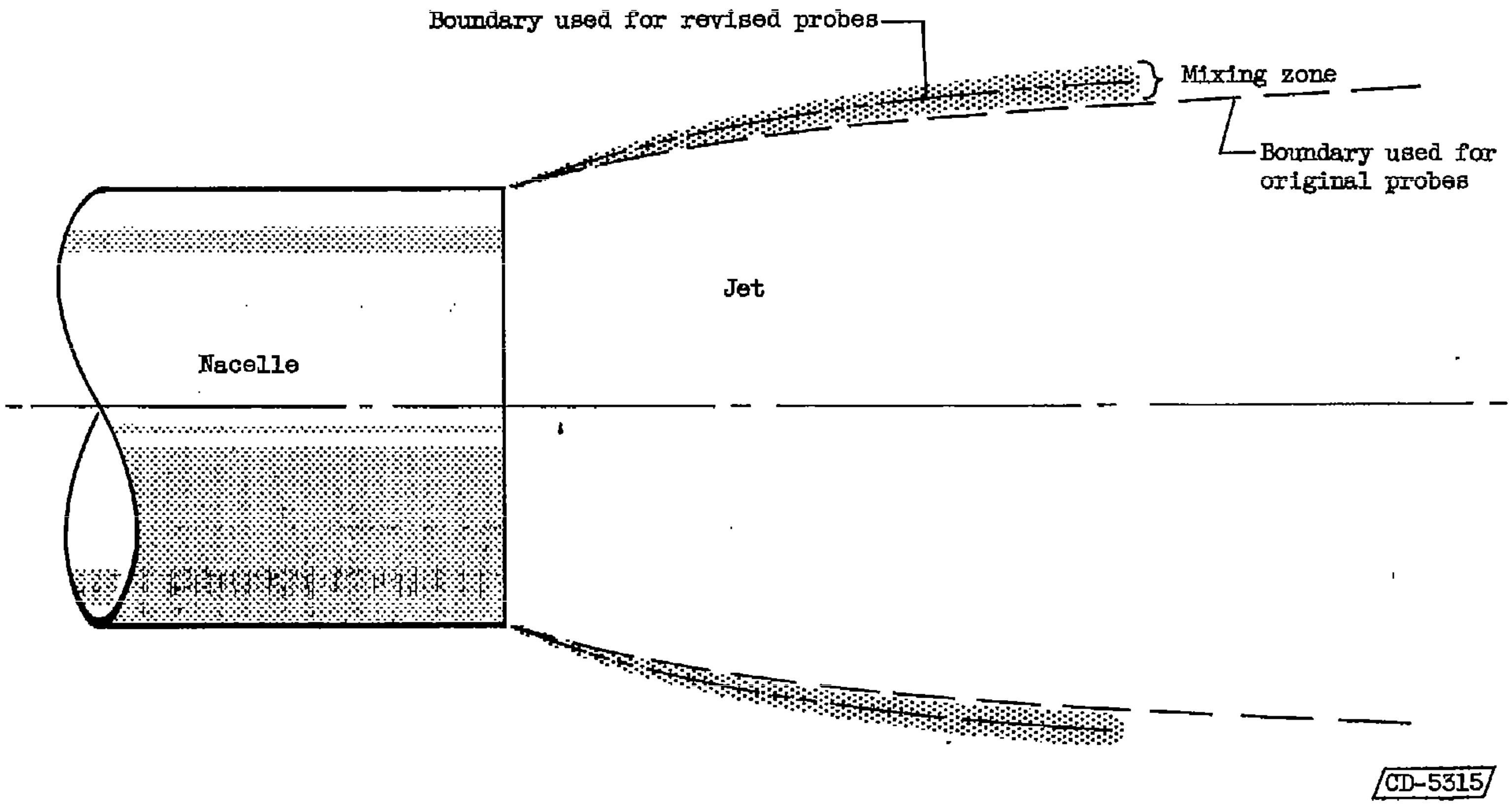

Figure 4. - Jet boundaries used to compute hole spacings in perforated probes. Free-stream Mach number, 3.0; jet-exit static-pressure ratio, 2.0.

4197

CO-3

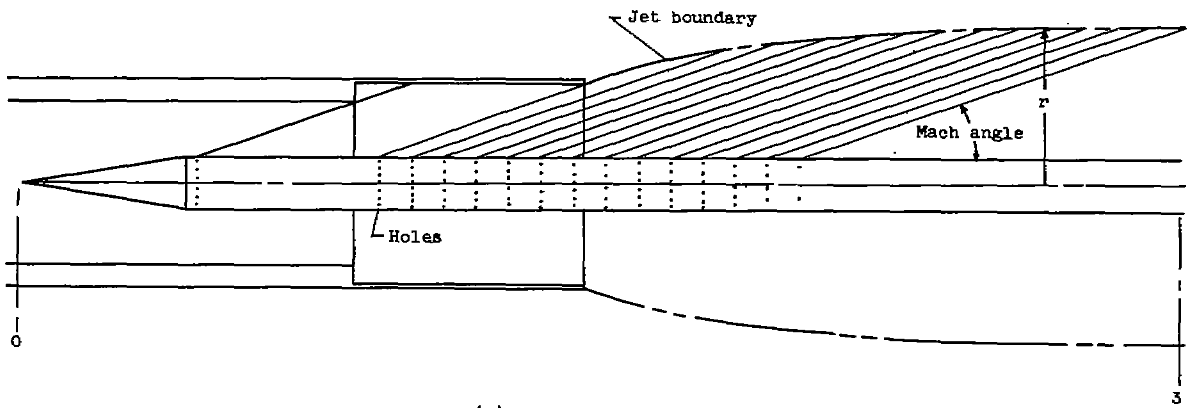

(a) Perforated probe.

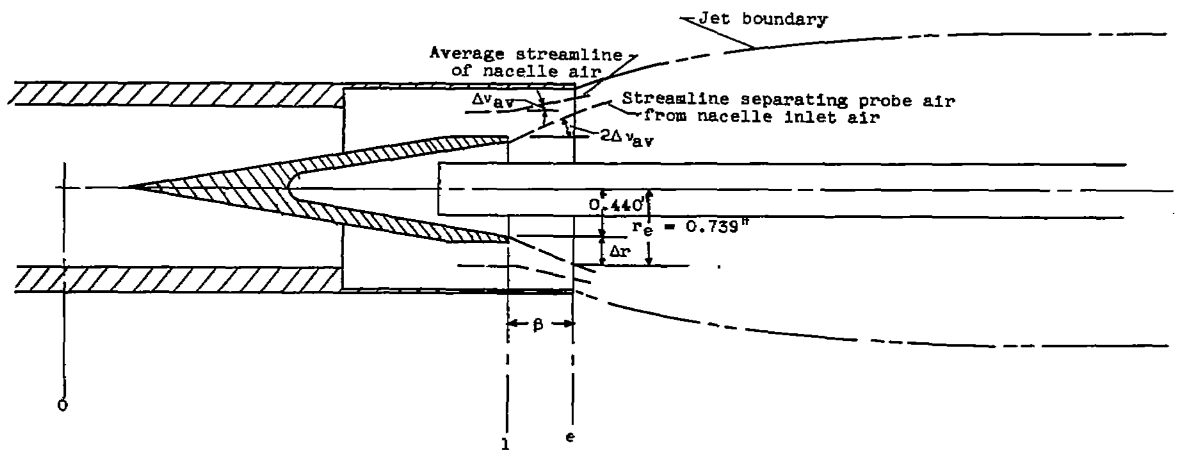

(b) Target probe.

Figure 5. - Probe designs.

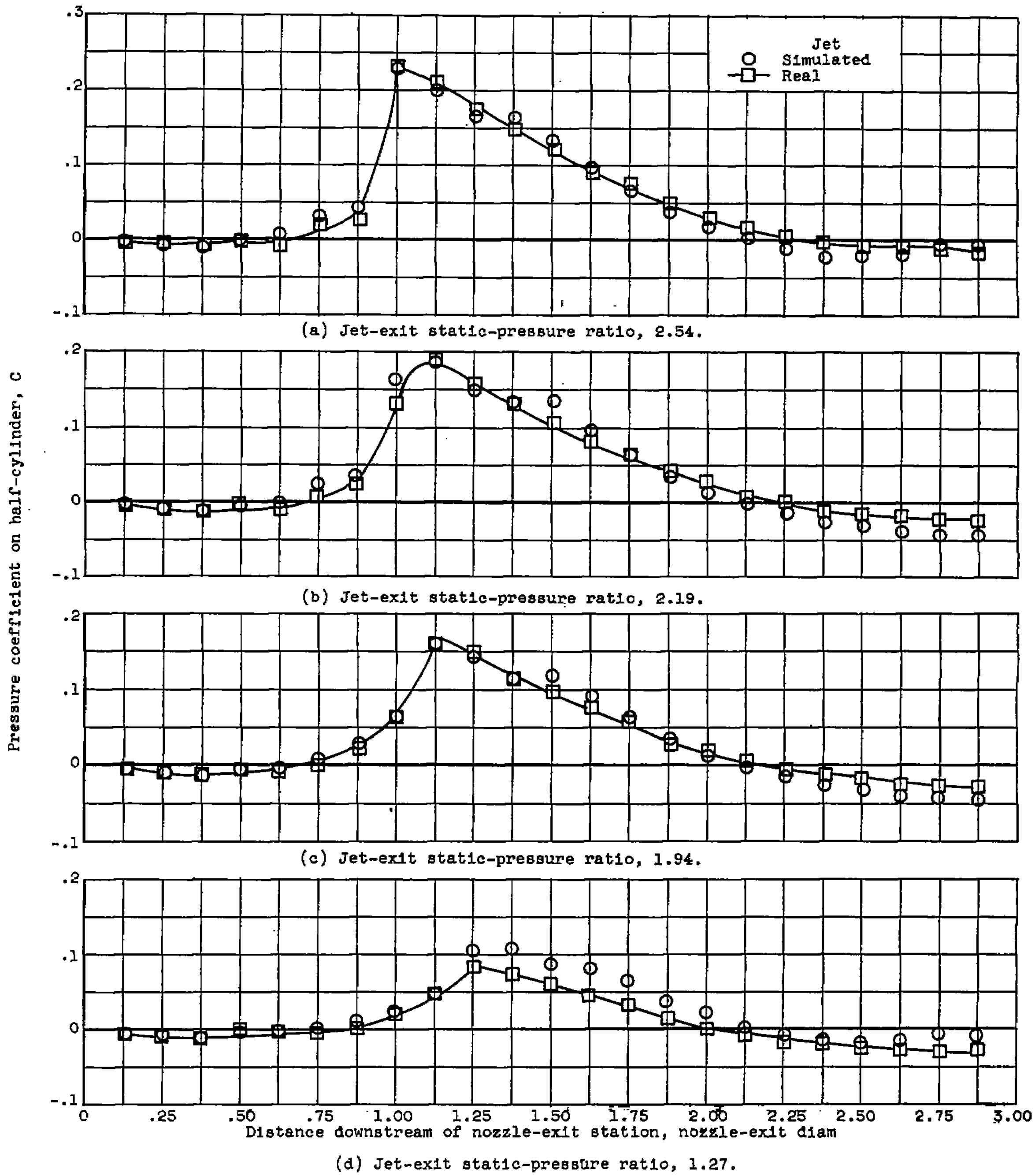

Figure 6. - Evaluation of target probe at free-stream Mach number of 3.0. Probe 5/16 exit diameter inside revised model.

4197

4197

CO-3 back

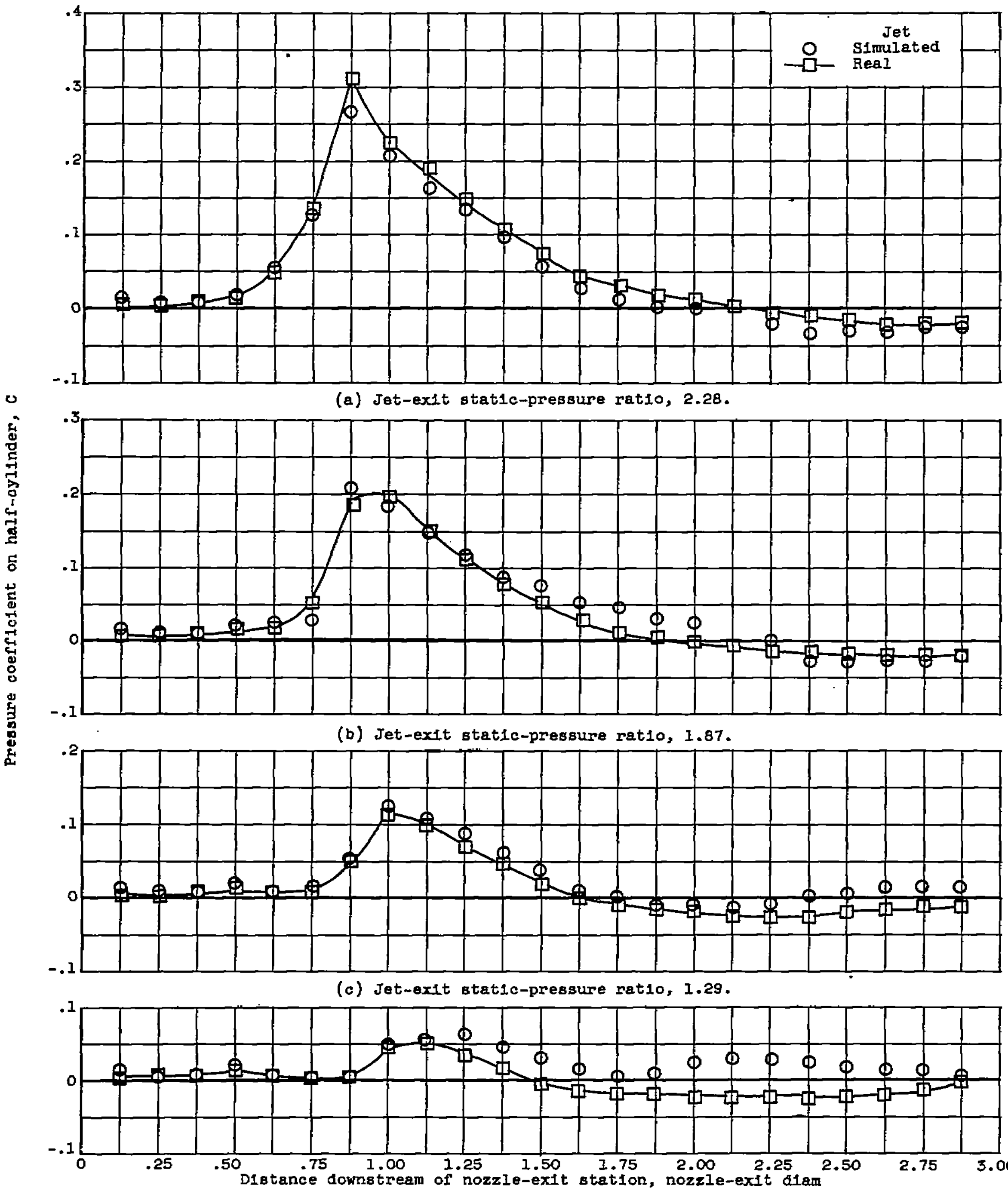

(d) Jet-exit static-pressure ratio, 1.00.

Figure 7. - Evaluation of target probe at free-stream Mach number of 2.5. Probe 5/16 exit diameter inside revised model.

4197

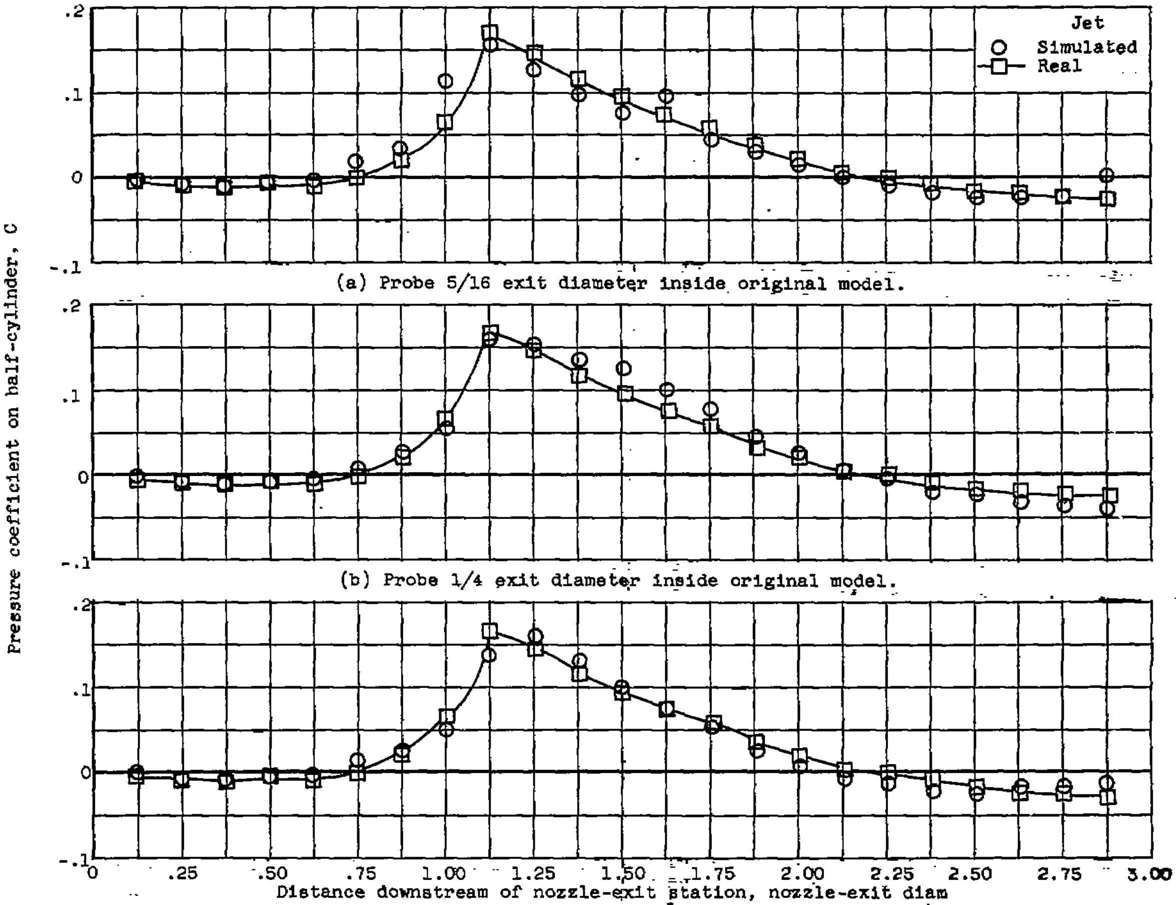

(c) Revised probe 5/16 exit diameter inside revised model.

Figure 8. - Development of target probe. Jet-exit static-pressure ratio, 1.94; free-stream Mach number, 3.0.

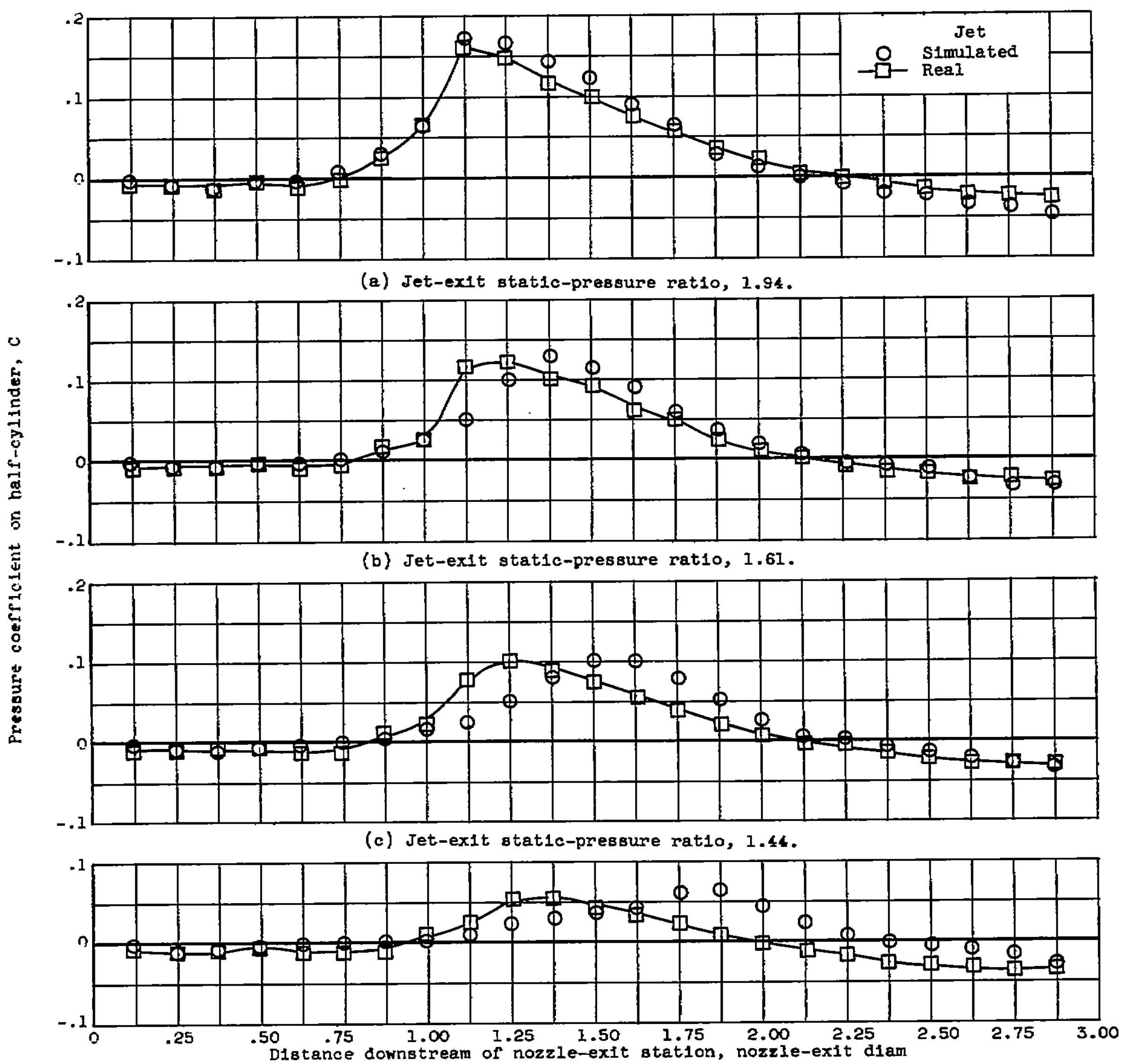

(a) Jet-exit static-pressure ratio, 1.94.

(b) Jet-exit static-pressure ratio, 1.61.

(c) Jet-exit static-pressure ratio, 1.44.

(d) Jet-exit static-pressure ratio, 1.05.

Figure 9. - Evaluation of perforated probe with holes normal to probe surface. Free-stream Mach number, 3.0; revised-probe shoulder 1.75 exit diameters inside revised model.

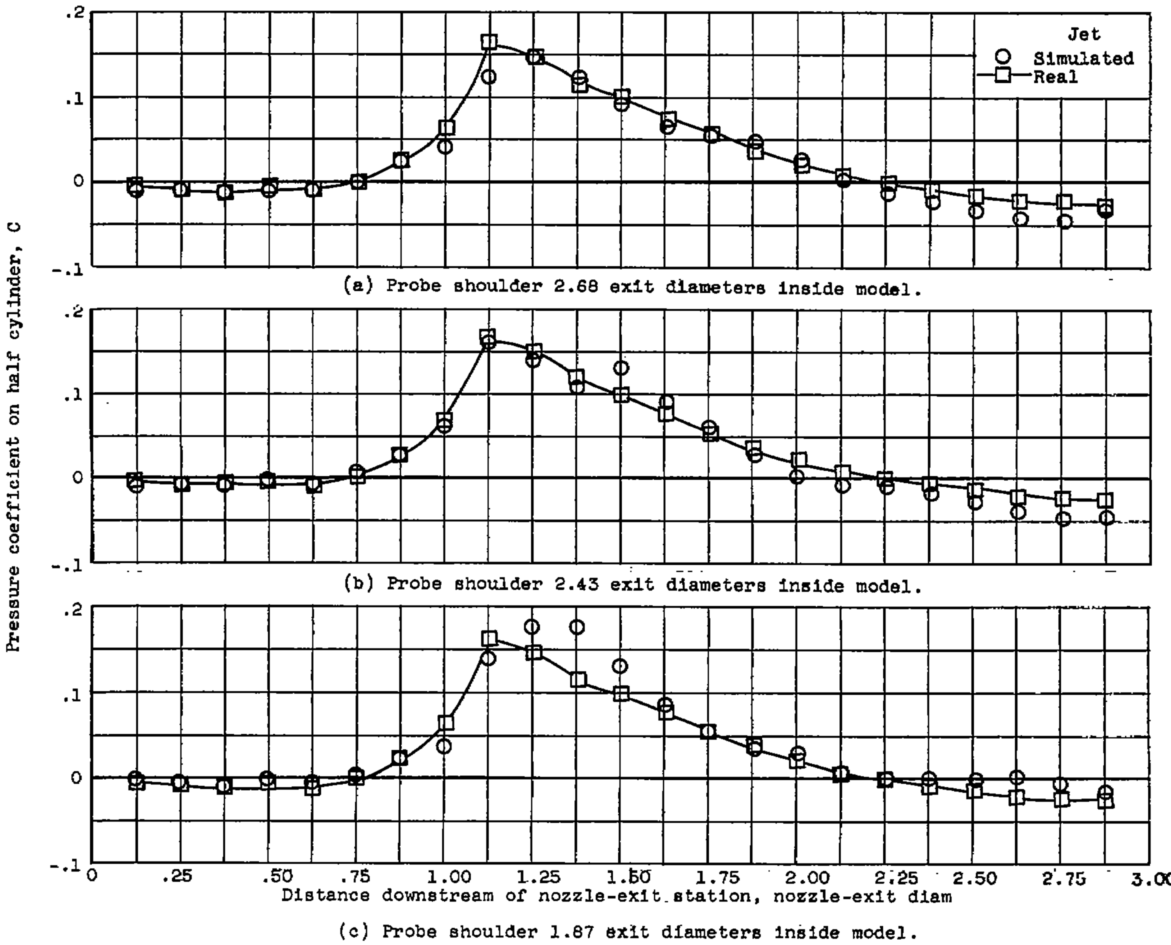

Figure 10. - Development of perforated probe with holes normal to surface. Jet-exit static-pressure ratio, 1.94; free-stream Mach number, 3.0.

4197

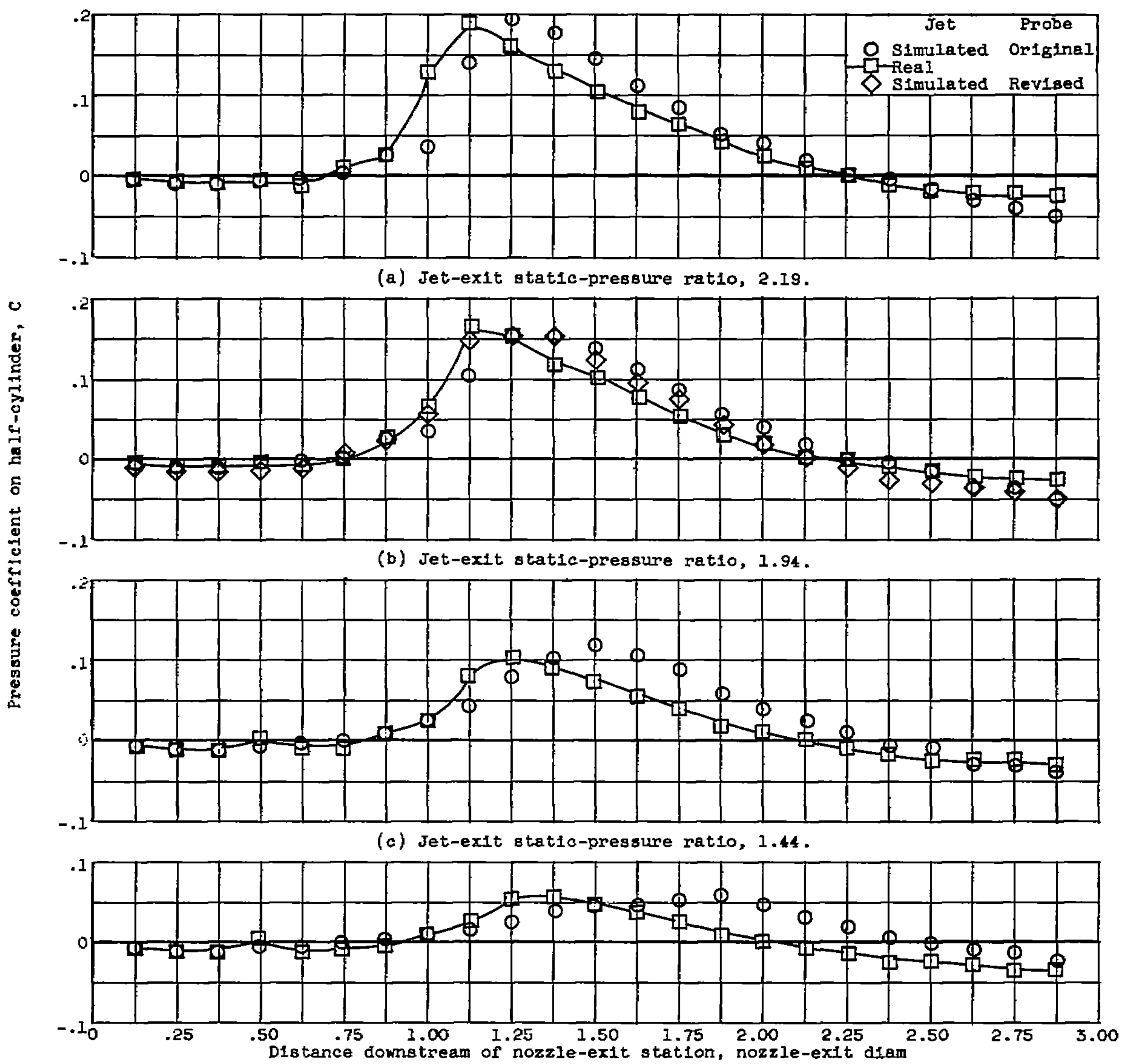

(a) Jet-exit static-pressure ratio, 2.19.

(b) Jet-exit static-pressure ratio, 1.94.

(c) Jet-exit static-pressure ratio, 1.44.

(d) Jet exit static-pressure ratio, 1.05.

Figure 11. - Evaluation of perforated probe with holes slanted 30° with respect to surface. Free-stream Mach number, 3.0; probe shoulder 2.68 exit diameters inside model.

4197

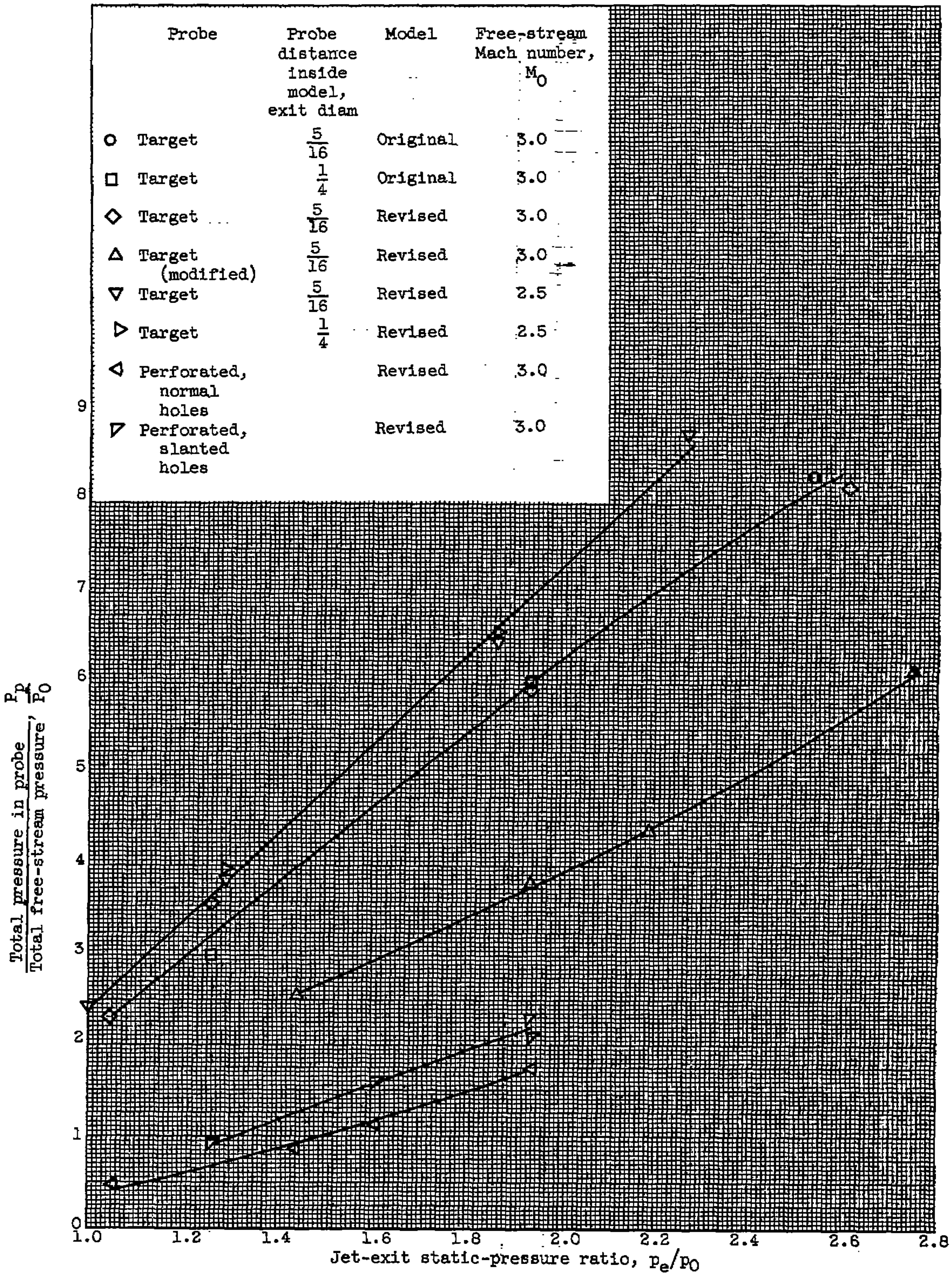

Figure 12. - Total pressure supplied to probe in jet simulation.

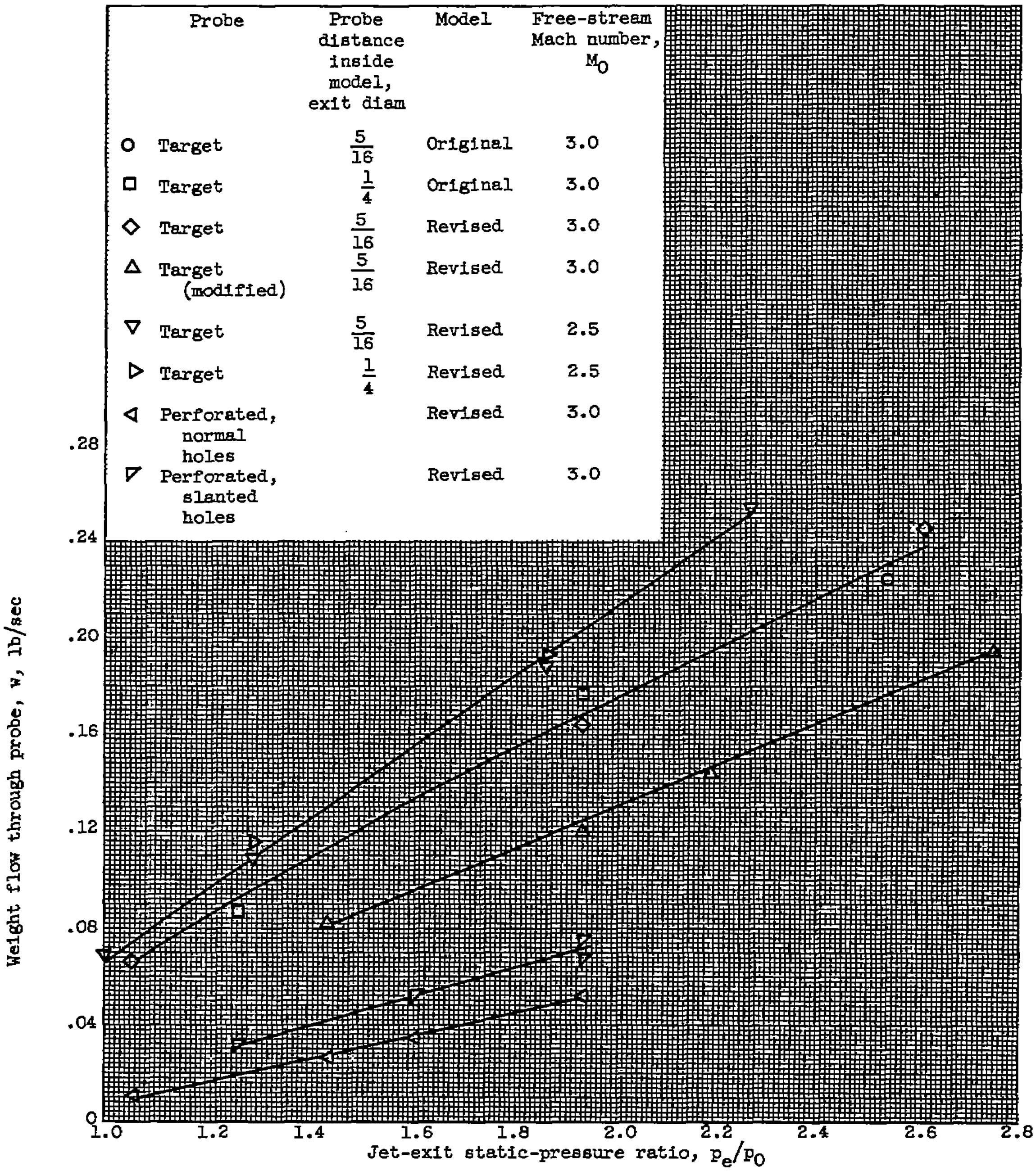

Figure 13. - Probe airflow required for jet simulation; weight flow parameter, $\frac{W\sqrt{T}}{P_pA_p}$; 0.34 for target probe; 0.39 for modified target probe; 0.41 for normal-hole and slant-hole probes.